

Metal–Organic Frameworks

Transistor-Based Work-Function Measurement of Metal–Organic Frameworks for Ultra-Low-Power, Rationally Designed Chemical Sensors

David W. Gardner,^[a, b] Xiang Gao,^[a, c] Hossain M. Fahad,^[a, d] An-Ting Yang,^[a, b] Sam He,^[c] Ali Javey,^[a, d] Carlo Carraro,^[a, b] and Roya Maboudian^{*[a, b]}

Abstract: A classic challenge in chemical sensing is selectivity. Metal–organic frameworks (MOFs) are an exciting class of materials because they can be tuned for selective chemical adsorption. Adsorption events trigger work-function shifts, which can be detected with a chemical-sensitive field-effect transistor (power \approx microwatts). In this work, several case studies were used towards generalizing the sensing mechanism, ultimately towards our metal-centric hypothesis. HKUST-1 was used as a proof-of-principle humidity sensor.

The response is thickness independent, meaning the response is surface localized. ZIF-8 is demonstrated to be an NO₂-sensing material, and the response is dominated by adsorption at metal sites. Finally, MFM-300(In) shows how standard hard–soft acid–base theory can be used to qualitatively predict sensor responses. This paper sets the groundwork for using the tunability of metal–organic frameworks for chemical sensing with distributed, scalable devices.

Introduction

Metal–organic frameworks (MOFs) are porous crystalline materials made up of metal nodes connected by organic linkers with thousands of known structures. The tunability of MOFs makes them attractive for chemical sensing in which the selectivity is a figure of merit. One of the most promising avenues for chemical sensing with MOFs is by work-function measurement. An advantage of this sensing mode is that work-function responses are available to all MOFs, unlike other modes, such as luminescence^[1] or conductivity,^[2–6] which can be applied to a limited number of available MOFs.

The mechanism for adsorbate-induced work-function changes are well understood for materials like metals,^[7,8] the

electronic structure of which can easily accommodate a change in electron concentration, but the addition or removal of an electron in a MOF is not as straightforward. One heuristic is that work-function responses are correlated with heat of adsorption, which makes work-function responses highly MOF–analyte specific so that a framework could be designed to target a particular analyte.^[9] In comparison, other modes such as mass change do not necessarily discriminate towards strong adsorption, especially if the analyte is dilute. For instance, our comparison of literature reports for the heat of adsorption of various alcohols on HKUST-1 correlates with the marginal work-function change per alcohol adsorbed.^[10,11] Another heuristic is that the work-function response depends to a large degree on the metal, which Davydovskaya et al. showed by using a Kelvin probe microscope with a series of M-btc MOFs, in which M = Co, Ni, Al, Cd, to a series of analytes^[12] (the corresponding experiment with various linkers has not been performed yet). However, a MOF's high affinity for an analyte is not necessarily enough to provoke a work-function shift. For instance, ethylene-diamine-appended Mg-MOF-74 has only a 15 mV work-function shift to 5000 ppm CO₂^[13,14] despite a binding energy on the order of 1 eV.^[15]


Unfortunately, the direct measurement of work function is not scalable because of the size of the sensors required (e.g., a Kelvin probe). However, indirect measurement of work function with a bulk silicon chemical-sensitive field-effect transistor (CS-FET) can leverage the same sensing characteristics but with a much smaller size, lower cost, and lower power (on the order of microwatts).^[16] These devices are advantageous over other work-function-based sensors (e.g., silicon nanowires or metallic nanostructures^[17,18]) because the bulk silicon is practi-

[a] D. W. Gardner, X. Gao, Dr. H. M. Fahad, A.-T. Yang, Prof. A. Javey, Prof. C. Carraro, Prof. R. Maboudian
Berkeley Sensor & Actuator Center, University of California, Berkeley
403 Cory Hall, Berkeley, CA, 94720 (USA)
E-mail: maboudia@berkeley.edu

[b] D. W. Gardner, A.-T. Yang, Prof. C. Carraro, Prof. R. Maboudian
Department of Chemical and Biomolecular Engineering
University of California, Berkeley, 201 Gilman Hall
Berkeley, CA, 94720 (USA)

[c] X. Gao, S. He
Department of Chemistry, University of California, Berkeley
420 Latimer Hall, Berkeley, CA, 94720 (USA)

[d] Dr. H. M. Fahad, Prof. A. Javey
Department of Electrical Engineering and Computer Sciences
University of California, Berkeley, 253 Cory Hall, Berkeley, CA, 94720 (USA)

 Supporting information and the ORCID identification number(s) for the author(s) of this article can be found under:
<https://doi.org/10.1002/chem.201902483>.

cally inert unless functionalized, whereas other structures tend to have very poor selectivity. In addition, bulk silicon provides a more manufacturable platform for, for example, distribution as part of an Internet-of-Things sensor array.

The CS-FET sensing mechanism is facilitated by the modulation of an ultrathin charge inversion layer in silicon by work-function change in the sensing layer. The inversion layer is made as thin as a few angstroms with proper doping and substrate biasing conditions, thus providing a very sensitive response.^[19] An optical image, a cartoon schematic, and the sensing mechanism for the device are given in Figure 1.

In this work, we show how MOFs can be integrated with the CS-FET to yield high-performance gas sensors, and discuss our hypothesis that work-function responses are dominated by the metal rather than the linker to guide future sensor development. Work-function measurements of MOFs are a sensitive means to measure adsorption at MOF surfaces, although these measurements lack the specificity of spectroscopic experiments.

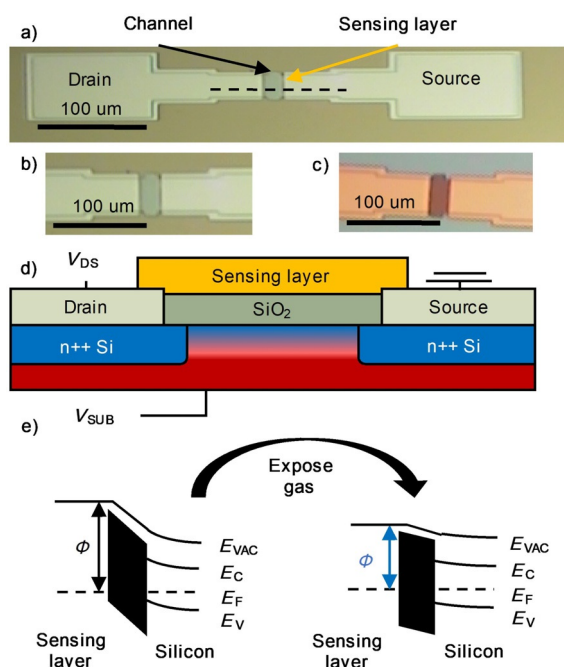


Figure 1. Chemical-sensitive field-effect transistor (CS-FET) and its operation. (a) Top-down optical image of the device, showing the source and drain electrodes separated by a channel. An arbitrary sensing layer is sketched. (b) Optical image of the channel before MOF deposition. (c) Representative optical image of the channel after MOF deposition (in this case, HKUST-1). (d) A cartoon cross-section of the dashed line in (a). The drain-source voltage V_{DS} , and the substrate voltage V_{SUB} (with respect to ground) are marked. (e) Sensing mechanism:^[22] when a gas adsorbs to the sensing material, its work function (ϕ) shifts, inducing changes in the band bending of the underlying silicon.

Results and Discussion

HKUST-1 sensing film

For a proof of principle, the first MOF presented for integration with the CS-FET is HKUST-1 (Figure 2a) because it can be used

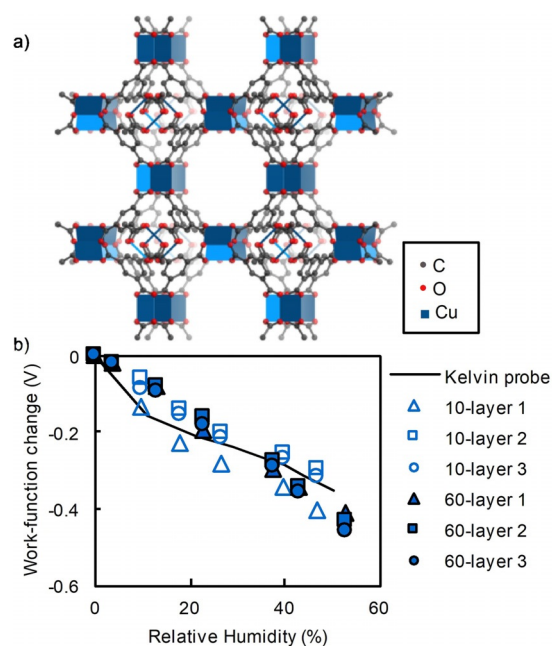


Figure 2. (a) Crystal structure of HKUST-1. (b) Calculated work-function change for the HKUST-1 sensing material compared to the value measured by a Kelvin probe,^[11] showing excellent agreement for all six sensors studied.

to resolve two questions about the sensing material: 1) How does the HKUST-1 CS-FET sensing response correlate with measured values on a Kelvin probe for the same exposure? 2) What is the impact of sensing layer thickness on the measured work-function change? In other words, is the response a bulk or surface-localized phenomenon? The first question was addressed by using literature data for the Kelvin probe response^[11] and comparing with our results. The second question was addressed by growing HKUST-1 in a cyclical or "layer-by-layer"^[23–25] manner directly on the CS-FET with 10 and 60 cycles.

The thicknesses of the 10-cycle and 60-cycle films as measured by AFM are approximately 60 nm and 250 nm, respectively, in good agreement with previous preparations.^[23,24] X-ray diffraction patterns of the synthesized films are given in Figure S2 (Supporting Information). The diffraction peaks are in good agreement with previous characterization of these films.^[23] The peaks of the layer-by-layer samples are a bit wider than those of powders, which is expected given the low-temperature synthesis.^[23,24] The low crystallinity may not be a problem for work-function based sensing, which some have proposed takes place at defect sites.^[9]

Representative sensor responses to humidity are given in Figure S3 (Supporting Information). The recovery to humidity is slow because of the inherent hysteresis for water absorption in HKUST-1^[26] and, possibly, the interference from the SiO₂ gate dielectric. The work-function change was calculated by using the method in the experimental section. We emphasize that the only fit parameter is the work-function change.^[19] A representative I_{DS} – V_{SUB} plot used for work-function shift calculation is given in Figure S4 (Supporting Information), where I_{DS} is the source-drain current and V_{SUB} is the substrate voltage as in

Figure 1. The calculated work-function change for three 10-cycle devices and three 60-cycle devices is given in Figure 2b overlaid with literature results obtained for HKUST-1 on a Kelvin probe.^[11] The calculated change in work function is in excellent agreement with the measured result for the 10- and 60-cycle devices, confirming that the change in work function of the MOF modulates the current.

The magnitude of the response is found invariant with the thickness of the MOF film. Therefore, the response is a near-surface-localized phenomenon. This conclusion is supported by the electrically insulating nature of MOFs, so a potential difference should not be felt many unit cells away. HKUST-1 proves to be insensitive to many interferants, including H₂, CH₄, H₂S, SO₂, CO₂, NH₃, and NO₂ (Figure S5, Supporting Information).

One variable of MOF work-function response is defect concentration, that is, MOFs that have more defects could give greater responses because the framework would more easily incorporate a guest into the physical and electronic structures.^[9] We are unable to quantitatively compare the defect concentration in the 10- and 60-cycle sensors, but based on previous preparations, we expect that the bottom layers of the film do not change much after several cycles, and so we expect that the defect concentration should be similar in both.^[24]

Figure S6 (Supporting Information) displays an overlay of the work-function response of HKUST-1 to H₂O with the adsorption isotherm of the same. The response is strongest in the low humidity regime when the most favorable sites, on the open metal sites of HKUST-1, are occupied, suggesting a metal-centric mechanism. The mechanism for response at higher relative humidities, when the open metal sites are completely saturated, is less clear. It is known that HKUST-1 expands when it absorbs water,^[27] which may lead to a structural change that could affect the surface dipoles, leading to a work-function change. More work is needed to understand the mechanism for work-function response at intermediate relative humidity ranges.

ZIF-8 humidity sensing

HKUST-1 is not an ideal sensing material because of its inherent instability in humidity.^[28] A MOF based on Zn-N linkages rather than Cu-O linkages is expected to be more robust per hard-soft acid base theory.^[29] One such MOF is ZIF-8 (Figure 3a). This MOF is deposited with a solvothermal method.^[30] X-ray diffraction pattern of the as-prepared thin film is provided in Figure S2 (Supporting Information), and compares well with previous characterization of these films.

ZIF-8 has a large response to humidity (Figure 3b). The response and recovery occurs within seconds of the change in relative humidity. The large response occurs despite the hydrophobic nature of the interior cavities, computational studies of which suggest that pressures of several MPa are needed to force water molecules inside.^[31] Therefore, the response must be from the surface of the MOF that would be in contact with the CS-FET gate. There are surfaces of the ZIF-8 crystals ex-

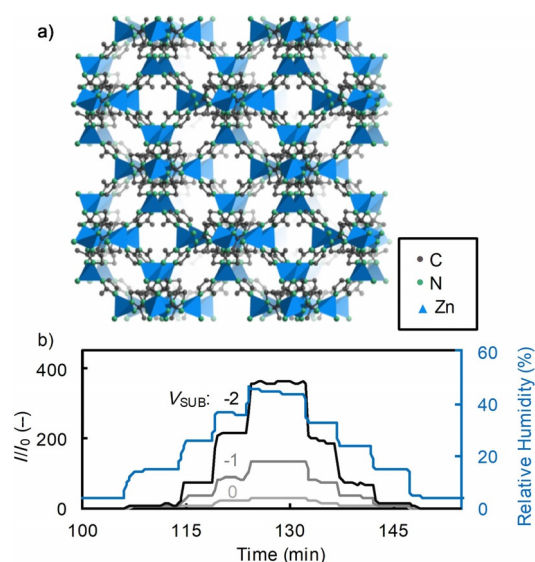


Figure 3. (a) Crystal structure of ZIF-8. (b) Normalized humidity response for a CS-FET functionalized with ZIF-8 for varied V_{SUB} .

posed to the atmosphere and in contact with the gate because of the nonconformal coating of the ZIF-8 sensing layer^[30] (see Figure S7b–d in the Supporting Information for optical image, SEM image, and cartoon schematic of ZIF-8 sensing film). Water molecules do not need to penetrate through the bulk of the crystal, but can adsorb on ZIF-8 surfaces that are capacitively coupled with the underlying silicon channel.

The response to humidity of ZIF-8 is uniquely identified as a work-function response rather than a conductometric response of ZIF-8 by comparing the change in current at various V_{SUB} values (Figure S8, Supporting Information). The change in current depends on the magnitude of V_{SUB} , but if the mechanism was conductometric, then there should be no dependence. We also measure the current through two arbitrary points on a surface with ZIF-8 film using a probe station at 3 V with ambient relative humidity at 50% and find less than 0.01 μA current, whereas typical drain-source current values are several μA .

X-ray photoelectron spectroscopy (XPS) was employed to investigate the near-surface composition of the MOF. The results shown in Figure 4 and Table 1 indicate that the surface of the ZIF-8 films are rich of zinc, with the surface termination being oxygen as hydroxyl or water, in good agreement with others' characterization^[32] showing a hydrophilic exterior. Zinc salts are extremely hydrophilic, so the sensing response to humidity is consistent with the XPS results.

To investigate the relationship between metal and linker for sensing response, we prepared a sensor with a dilute zinc acetate sensing layer. The zinc acetate sensors also have a very strong response to humidity (Figure S9, Supporting Information). However, the recovery is much slower in the zinc acetate sensor because of the formation of zinc hydrate salts in the high humidity, causing the sensor to approach a new baseline after the exposure. The crystalline framework of ZIF-8 inhibits the formation of these salts so that the sensor can recover to

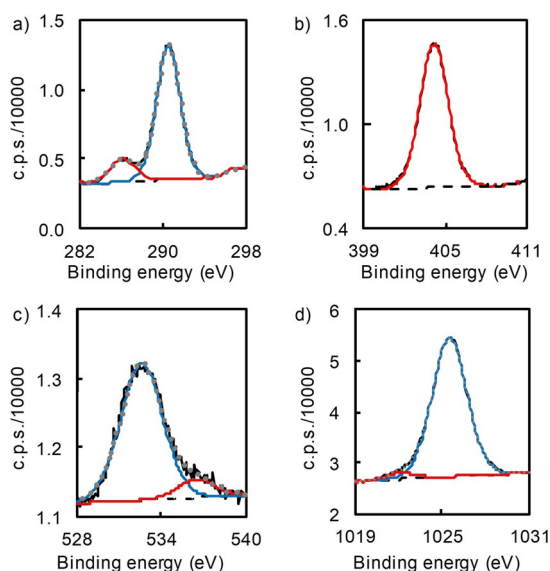


Figure 4. X-ray photoelectron spectra for ZIF-8 sensing film. (a) C 1s, (b) N 1s, (c) O 1s, (d) Zn 2p^{3/2} regions. Solid black line represents the signal; dashed black line represents background; red and blue lines represent fit to specific peaks; dashed gray line represents fitted envelope.

Table 1. Atomic ratios determined by X-ray photoelectron spectroscopy for ZIF-8 sensing films in this work on silicon.

Element	Zn	N	C	O
This work	1.0	1.7	4.1	0.4
Stoichiometry	1.0	4.0	8.0	0.0

the original baseline within seconds (Figure S10, Supporting Information). This indirect test shows how the metals may control the magnitude of the response, but the crystalline framework of the MOF is still needed for a robust response.

ZIF-8 NO₂ sensing

Figure 5 shows the response of a CS-FET with ZIF-8 sensing film to NO₂ in three different humidity environments, with the lowest humidity level repeated as the final measurement when measured at $V_{\text{SUB}} = 0$ V. The magnitude of the response increases with increasing concentration in NO₂ and increasing humidity. When the change in work function is plotted against the NO₂ concentration, a first-order relationship with NO₂ is observed (Figure S11, Supporting Information).

The magnitude of the response over the duration of the exposure (three minutes in each case) was repeatable for the lowest humidity window. An on-stream humidity sensor verified that humidity remained within 1.5% of the target value during the exposure; thus, the response can be uniquely assigned to the NO₂ in the atmosphere (see Figure S12, Supporting Information, for relative humidity data from on-stream humidity sensor).

The response–recovery times are much slower for NO₂ exposures than humidity. Although the cross-sensitivity to humidity

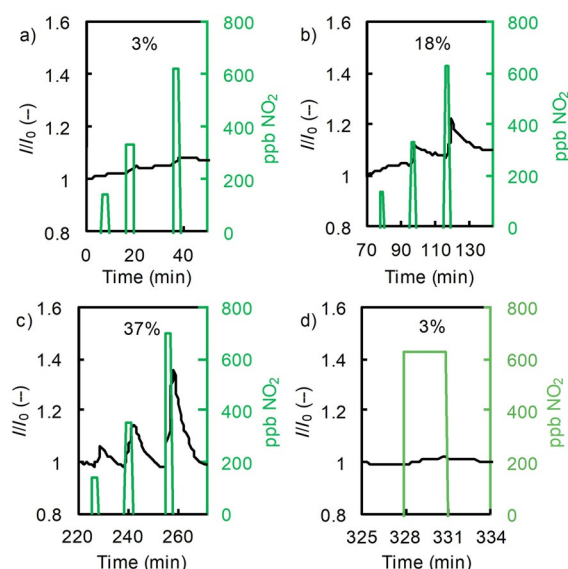


Figure 5. (a–d) Normalized response for a CS-FET functionalized with ZIF-8 to NO₂ at 3%, 18%, 37%, and a repeat of 3% relative humidity, respectively, indicated by the number at the top of each Figure. Current was renormalized at the beginning of each time window.

may seem like a problem for using MOF work-function sensing, in practice the humidity response would be compensated for with a parallel humidity sensor (e.g., HKUST-1 above).^[16] ZIF-8 is insensitive to a wide variety of interferants, including H₂, CH₄, H₂S, CO₂, SO₂, and NH₃ (Figure S13, Supporting Information).

Our sensing results are well complemented by the recent characterization of ZIF-8 in NO₂ by Bhattacharyya et al.^[33] In their spectroscopic work, they find that the first defects from NO₂ in dry air come from H-abstraction from the linker and functionalize the linker with NO₂. The reaction forms HNO₂ as a byproduct. Once HNO₂ forms, it can protonate the linker and form an inorganic nitrate with the metal.

In dry air (Figures 5a,d), the reaction between NO₂ and the framework occurs primarily on the linker. These reactions are mostly irreversible, given the strength of the N–C bond, so the response does not recover. In humid air (Figures 5b,c) the stream of gas is nominally H₂O and NO₂, but actually contains HNO₂ and HNO₃ because of the reactivity of NO₂ in humid air. These acids can immediately form inorganic nitrates.^[33]

We observe greater work-function shifts from NO₂ exposures that occur in higher relative humidity environments. These adsorption events are primarily the NO_x[−] at zinc metal sites after the linker becomes protonated rather than bond-making with the linker.^[33] This is strong evidence that targeting adsorption at metals rather than linkers is a useful heuristic for designing MOF chemical sensors.

There is a recovery in work function after the NO₂ exposure in humid air. Given the ease with which zinc-based MOFs exchange ligands, it is plausible that the framework is recovering from the inorganic nitrate exposure. X-ray diffraction pattern of the film exposed to NO₂ is given in Figure S2 (Supporting Information) and shows only a slight decrease in diffraction intensity. More advanced characterization methods, such as in

situ XRD or FTIR capable of dosing humid NO_2 , are needed to unambiguously explain the recovery. The surprising results agree with Bhattacharyya's characterization showing reasonable stability of ZIF-8 in humid NO_2 .^[33]

The ZIF-8 NO_2 sensing experiments show that there are other uses for work-function measurements of MOFs. Those studying MOF stability could benefit from the sensitivity of the technique to measure the extent of- and rate of- reaction of the framework when exposed to harsh gases, since traditional methods to do so are quite laborious.^[34]

MFM-300(In) chemical sensing

As a final demonstration of a metal-centric hypothesis, we test the carboxylate-containing MOF "MFM-300(In)". We choose this MOF because it has carboxylate linkers and has been reported to have good sensing properties in humidity,^[35] suggesting it to be promising as a practical sensing material. MFM-300(In) responds to a base, NH_3 , whereas there was no response to NO_2 (Figure 6) in 3% relative humidity air. Although this exact

sensitivity to humidity,^[35] we found practically no response to 10 ppm SO_2 and a large work-function response to humidity. These experiments show that the work-function responses have little correlation with capacitance responses. Minimizing the work-function response to humidity will be a challenge for utilizing metal-organic frameworks as a sensing material on the CS-FET.

Although we have focused on the functional groups on the linker, the response is still metal dominated, because the chemistry of the ligating group in a stable MOF is determined by the metal by the hard-soft acid-base theory. The sluggish recovery of MFM-300(In) to 1 ppm NH_3 is not ideal, but practically speaking there are many sensing applications where sensors are needed just once, for example, a safety badge that alerts a user to a toxic gas in their environment. The responses described here are clearly distinguished from the bare sensor (i.e., exposed oxide) sensing responses, provided in Figure S15 (Supporting Information).

Conclusions

In this work, several well-characterized MOFs were integrated with a chemical-sensitive field-effect transistor and their work-function responses are explained by using a metal-centric hypothesis. The MOF HKUST-1 shows 1) the sensing response on the device is predicted by experiments that directly measure the work-function change, and 2) the response is surface-localized. The MOF ZIF-8 supports finding 2) through its large humidity response when water molecules adsorb at the zinc-rich surface. The ZIF-8 sensors respond most strongly and recover most when exposed to NO_2 in humid rather than dry air. These two findings are complementary to a separate literature spectroscopic experiments that showed that humid NO_2 attacks metal sites and dry NO_2 attacks the linker.^[33] Lastly, the MOF MFM-300(In) was used as a final example of how work-function responses can be predicted based on chemical resistance rules arising from the metal chemistry and hard-soft acid-base chemistry.

The work-function shift of MFM-300(In) to NH_3 is quite small compared to the NO_2 response of ZIF-8. So far we do not yet understand what governs the magnitude of a particular MOF work-function response to a particular gas, but the chemical resistance rules are a reasonable starting point for what will and will not respond.

These experiments provide guidelines for selection of MOF-analyte combinations for the emerging field of work-function-based sensing on chemical-sensitive field-effect transistors for ultra-low-power sensing. There is proportionality for the HKUST-1 and H_2O , ZIF-8 and H_2O , and ZIF-8 and NO_2 , so this sensing mode has promise for quantitative sensors once properly calibrated.

We generally observe that the sensitivity of MOF work-function shifts to chemical adsorption events is mediocre compared to that of metals.^[16,19] To mitigate this, the CS-FET platform has a built-in response multiplier with its substrate voltage V_{SUB} .

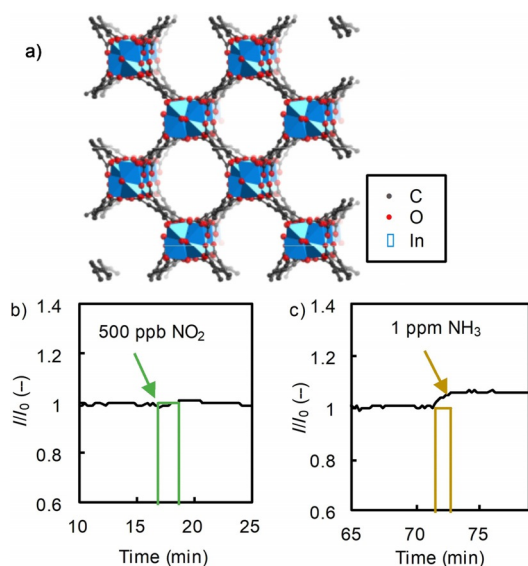


Figure 6. (a) Crystal structure of MFM-300(In). (b) Sensing response of MFM-300(In) sensing layer to 500 ppb NO_2 . (c) Sensing response of MFM-300(In) sensing layer to 1 ppm NH_3 .

system has not yet been studied in situ spectroscopically, a neutron diffraction study of MFM-300(Al) shows NH_3 binding occurring at the metal site.^[36] Separate capacitance measurements of MFM MOFs show that there is negligible NO_2 adsorption in the concentration range we study.^[35] The imidazole-containing framework ZIF-8 did not respond to NH_3 (Figure S13, Supporting Information), but as described above, does respond to NO_2 . These responses are in agreement with the predictions of well-known chemical resistance rules.^[37]

The work-function response of MFM-300(In) to SO_2 and humidity is given in Figure S14 (Supporting Information). Although others have found that the material capacitance has a high sensitivity to SO_2 (< 75 ppb detection limit) and minimal

These findings suggest that work-function monitoring of MOFs is a sensitive, if nondescript, measure of a MOF stability in reactive environments. MOF stability experiments are challenging to do in situ because reactive environments (e.g., humidity and NO₂^[33] or SO₂^[38]) will etch the spectrometer windows; thus, ex-situ measurements prevail. A work-function probe such as the CS-FET or Kelvin probe is a sensitive means to measure how the surface electronic structure responds to reactive environments.

Several open questions remain about work-function responses. Re-examining Figure S6 (Supporting Information), which plots the work-function response of HKUST-1 to H₂O vs. an adsorption isotherm for the same, the work-function response continues well past the point at which open metal sites would be filled and nearly all adsorption is taking place through adsorbate-adsorbate interactions inside the pores. It is not clear how these pore-filling guests are able to modulate the work function. A related question is why the work-function response can be enhanced by modifying the active site with functionalities appended on the linker.^[9] The magnitude of the work-function shift is also not yet understood with only empiricism used to describe the response. Further work is needed to understand more fully the origins of the response, so that sensors can be prepared with greater predictive power for sensor performance.

Experimental Section

Methods and instruments

Sensors were fabricated according to standard microfabrication methodologies, and in-depth details on the device fabrication can be found in Ref. [19]. Prior to depositing the metal-organic framework layer, the devices were cleaned with a 10-min sonicating bath of acetone, then isopropyl alcohol, dried in N₂, and exposed to UV light and ozone for 10 min. This cleaning process removes the protective photoresist layer and any residual organics so that the channel is pristine. A coupon of <100> silicon follows the devices during the procedure for sensing film characterization.

The MOF HKUST-1 was deposited by using a layer-by-layer method^[1,23–25,30] on devices cleaned by successive rinsing in acetone, isopropyl alcohol, and water and a 15-min UV-light and ozone treatment. The device was alternately immersed in an ethanolic solution containing the metal ion, as 50 mM copper acetate, rinsed in fresh ethanol, immersed in an ethanolic solution containing the linker, as 100 mM 1,3,5-benzene-tricarboxylic acid. The device and the partner silicon coupon were given 10 or 60 cycles. The MOFs were then submerged in a series of two ethanol baths for 1 h each to remove unreacted precursors and activated at 120 °C under a low-pressure nitrogen environment ($P < 1$ torr, 50 sccm N₂) to remove solvent molecules.

The MOF ZIF-8 was prepared with a solvothermal method in methanol, 50 mM in zinc nitrate and 100 mM in 2-methylimidazole.^[30] The devices were placed in a bath containing the synthesis broth at room temperature for 1 h, then transferred into a fresh-solution bath for another hour, and finally into a third bath for an additional hour. The MOF was then submerged in a series of two ethanol baths for one hour each to remove unreacted precursors and activated at 120 °C under a low-pressure nitrogen environment ($P < 1$ torr, 50 sccm N₂) to remove solvent molecules.

The MOF MFM-300(In) was prepared by a standard method.^[39] The crystals were dropcast over the surface of the device in acetone and activated in gentle heating.^[40] A dropcast method was needed because a thin film could not be prepared on the device. In general, larger responses were obtained when the sensing film was deposited by direct growth rather than dropcast, likely because of the better physical contact between the MOF and the gate dielectric.

The zinc acetate sensor was prepared by immersing a cleaned device in a 50 mM methanolic solution of zinc acetate for one hour followed by a rinse in a methanol bath. The device was gently rinsed in DMF and stored in vacuum.

It should be noted that although the sensing films cover the contacts as well as the gate, there is no effect on the electronics since the dominant resistance contributing to source-drain current is the channel.^[16,19] The MOF thin films deposited are insulating and carry negligible current, confirmed by measuring the resistance between two arbitrary points on the silicon coupon after MOF deposition with a standard probe station, showing > 100 M Ω resistance.

The structural, chemical, and topographic characterizations of the films were done on a silicon coupon that followed the device through the synthesis. X-ray diffraction patterns were recorded by using a Bruker AXS D8 Discover GADDS XRD diffractometer system with a grazing angle of 0.3° and a CuK α source. X-ray photoelectron spectra (XPS) were collected with an Omicron Dar400 system with an achromatic Al K α source. The ZIF-8 sensing specimen was prepared on a silicon coupon as described above with an additional activation bath in acetone and stored in vacuum overnight before loading into the XPS sample analysis chamber. Atomic force microscopy (AFM) was performed with a Bruker Icon in tapping mode. The resistance measurements conducted on a probe station were performed using a Keithley 2602 source-meter. Scanning electron microscopy was done using a Phenom Pro benchtop SEM at 15 kV beam energy.

All gas-sensing measurements were carried out in a walk-in fume hood. Devices were wire bonded to a 28-pin J-bend leaded chip carrier. A small-volume (~ 0.83 cm³) 3D printed housing, made of polylactic acid, consisting of a $\frac{1}{4}$ -inch gas inlet was used to cover the chip carrier. Synthetic dry air was used as diluent gas and was procured from Praxair Technology Inc. Synthetic air-diluted gas cylinders were purchased from MESA International Technologies Inc. at a calibrated concentration. Typical gas flow rates were from 1 to 100 sccm, and diluent (air) flow rate was 100–1000 sccm. Humidity was controlled by diverting the diluent through a bubbler filled with 18 M Ω cm water. Ambient temperature and humidity were monitored by commercial sensors purchased from Sensirion AG (models SHT2x and SHT3x). Gas delivery was controlled by mass flow controllers (Alicat Scientific Inc.). CS-FET sensors were biased by using a Keithley 428 current preamplifier, and the current signals were acquired using a LabVIEW-controlled data acquisition unit (National Instruments, NI USB-6259). All sensing data presented here were obtained at $V_{DS} = 3$ V and $V_{SUB} = 0$ V, unless otherwise noted.

For all experiments where gasses are dosed in a relative humidity environment, the flow rate of humid and dry air is adjusted to keep a constant relative humidity in the chamber.

The transistor design equation^[22] was used to estimate changes in work function of the sensing material, given in Equation (1):

$$I_{DS} = C_{ox} * \mu_n * \frac{W}{L} * V_{DS} * \left(V_G - V_T - \frac{1}{2} V_{DS} \right) \text{ when } \frac{1}{2} V_{DS} < (V_G - V_T) \quad (1)$$

in which I_{DS} is the current from source to drain, C_{OX} is the capacitance of the gate oxide, μ_n is the electron mobility, W is the width of the channel, L is the length of the channel, V_{DS} is the potential between the source and drain, V_G is the potential difference between the gate and the source, and V_T is the canonical “threshold voltage” that is characteristic for each channel–gate pair. Threshold voltage depends on the work-function difference between the material on the gate (in this work, the MOF sensing layer) and the underlying silicon because of the inherent electric field generated between two materials with different work functions.^[22] This working principle is supported by Figure S1 (Supporting Information), which shows a threshold voltage shift when 60 cycles of HKUST-1 are grown on a device. The data corresponding to “bare device” were recorded on a probe station when the ambient relative humidity was <10%, and the points corresponding to 60-cycle HKUST-1 were recorded after wire bonding to the same device and recorded in the gas sensing setup at <4% relative humidity environment.

The threshold voltage shift, ΔV_T with V_{SUB} applied is given in Equation (2):

$$\Delta V_T = \frac{\sqrt{(2\epsilon_s q N_{SUB})}}{C_{OX}} [(2\varphi_F - V_{SUB})^{0.5} - (2\varphi_F)^{0.5}] \quad (2)$$

in which ϵ_s is the dielectric constant for silicon, q is the charge of an electron, N_{SUB} is the doping of the body silicon ($\approx 8 \times 10^{14} \text{ cm}^{-3}$), and φ_F is the difference between the mid-gap and the Fermi energy level in the silicon body ($\approx 0.3 \text{ V}$ for this system). The dielectric properties of the MOF do not directly enter Equation (2) because they have already been considered as part of the threshold voltage in Equation (1). The quantity under the radical in Equation (2) can be thought of as the effective capacitance of the silicon substrate, while the terms in the square bracket can be thought of as changing the effective doping level in the silicon substrate.

Combining Equations (1) and (2) allows for the change in gate voltage, that is, the change in work function of the gate, to be estimated. If the current is equalized for two pairs of gate voltages and body voltages before and after a gas exposure, the change in gate voltage is given by Equation (3):

$$V_{G,1} - V_{G,2} = 0.177 * [(0.6 - V_{SUB,2})^{0.5} - (0.6 - V_{SUB,1})^{0.5}] \quad (3)$$

The factor of 0.177 comes from the prefactor in Equation (2) with the relevant values applied and assuming an effective oxide thickness of 3 nm.^[19,41] When extracting a work function from I_{DS} – V_{SUB} plots, a representative plot of which is given in Figure S2 (Supporting Information), at least three pairs of points were recorded along the line and averaged to yield a work function. These points were spaced at least $0.5 V_{SUB}$ apart on the “before” reading and points were used with the lowest V_{SUB} available. If Equation (3) was not possible because of such a large current change, then the work-function shift was estimated by using a nonlinear regression for the work-function shift, first fitting the pre-exposure data to acquire the prefactor and V_T , and then fitting only the work-function shift. Equation (3) is preferable because it is computationally less expensive and still gives values that are within 10% of the values obtained by regression.

Acknowledgements

We would like to thank the Industrial Members of the Berkeley Sensor & Actuator Center (BSAC) and National Science Foundation (grant no. 1903188) for their support of this project. A.J. acknowledges the Bakar Fellows Program for additional funding. Work at the Molecular Foundry was supported by the Office of Science, Office of Basic Energy Sciences, of the US Department of Energy under contract no. DE-AC02-05CH11231.

Conflict of interest

H.M.F. and A.J. declare competing financial interests in equity on shares of Serinus Labs, Inc.

Keywords: adsorption • gas sensing • metal–organic frameworks • surface chemistry • XPS

- [1] O. Shekha, J. Liu, R. A. Fischer, C. Wöll, *Chem. Soc. Rev.* **2011**, *40*, 1081.
- [2] M. G. Campbell, S. F. Liu, T. M. Swager, M. Dincă, *J. Am. Chem. Soc.* **2015**, *137*, 13780–13783.
- [3] M. G. Campbell, D. Sheberla, S. F. Liu, T. M. Swager, M. Dincă, *Angew. Chem. Int. Ed.* **2015**, *54*, 4349–4352; *Angew. Chem.* **2015**, *127*, 4423–4426.
- [4] L. Sun, M. G. Campbell, M. Dincă, *Angew. Chem. Int. Ed.* **2016**, *55*, 3566–3579; *Angew. Chem.* **2016**, *128*, 3628–3642.
- [5] T. C. Narayan, T. Miyakai, S. Seki, M. Dinca, *J. Am. Chem. Soc.* **2012**, *134*, 12932–12935.
- [6] S. Achmann, G. Hagen, J. Kita, I. M. Malkowsky, C. Kiener, R. Moos, *Sensors* **2009**, *9*, 1574–1589.
- [7] S. Å. Lindgren, L. Walldén, *Phys. Rev. B* **1980**, *22*, 5967–5979.
- [8] P. J. Goddard, R. M. Lambert, *Surf. Sci.* **1977**, *67*, 180–194.
- [9] I. Stassen, B. Bueken, H. Reinsch, J. F. M. Oudenhoven, D. Wouters, J. Hajek, V. Van Speybroeck, N. Stock, P. M. Vereecken, R. Van Schaijk, D. De Vos, R. Armeloot, *Chem. Sci.* **2016**, *7*, 5827–5832.
- [10] T. R. C. Van Assche, T. Duerinck, J. J. Gutiérrez Sevillano, S. Calero, G. V. Baron, J. F. M. Denayer, *J. Phys. Chem. C* **2013**, *117*, 18100–18111.
- [11] P. Davydovskaya, R. Pohle, A. Tawil, M. Fleischer, *Sensors Actuators B Chem.* **2013**, *187*, 142–146.
- [12] P. Davydovskaya, V. Pentyala, O. Yurchenko, L. Hussein, R. Pohle, G. A. Urban, *Sensors Actuators B Chem.* **2014**, *193*, 911–917.
- [13] V. Pentyala, P. Davydovskaya, M. Ade, R. Pohle, G. Urban, *Sensors Actuators B Chem.* **2016**, *225*, 363–368.
- [14] V. Pentyala, P. Davydovskaya, R. Pohle, G. Urban, O. Yurchenko, *Procedia Eng.* **2014**, *87*, 1071–1074.
- [15] S. Choi, T. Watanabe, T. H. Bae, D. S. Sholl, C. W. Jones, *J. Phys. Chem. Lett.* **2012**, *3*, 1136–1141.
- [16] H. M. Fahad, H. Shiraki, M. Amani, C. Zhang, V. S. Hebbbar, W. Gao, H. Ota, M. Hettick, D. Kiriya, Y.-Z. Chen, Y. L. Chueh, A. Javey, *Sci. Adv.* **2017**, *3*, e1602557.
- [17] N. Shehada, G. Brönstrup, K. Funka, S. Christiansen, M. Leja, H. Haick, *Nano Lett.* **2015**, *15*, 1288–1295.
- [18] R. Duś, E. Nowicka, R. Nowakowski, *Acta Phys. Pol. A* **2008**, *114*, S29–S47.
- [19] H. M. Fahad, N. Gupta, R. Han, S. B. Desai, A. Javey, *ACS Nano* **2018**, *12*, 2948–2954.
- [20] K. T. Butler, C. H. Hendon, A. Walsh, *J. Am. Chem. Soc.* **2014**, *136*, 2703–2706.
- [21] C. H. Hendon, A. Walsh, *Chem. Sci.* **2015**, *6*, 3674–3683.
- [22] C. C. Hu, *Modern Semiconductor Devices for Integrated Circuits*, Pearson Education, New York, **2009**.
- [23] V. Stavila, J. Volponi, A. M. Katzenmeyer, M. C. Dixon, M. D. Allendorf, *Chem. Sci.* **2012**, *3*, 1531–1540.
- [24] M. L. Ohnsorg, C. K. Beaudoin, M. E. Anderson, *Langmuir* **2015**, *31*, 6114–6121.

- [25] D. Zacher, O. Shekhah, C. Wöll, R. A. Fischer, *Chem. Soc. Rev.* **2009**, *38*, 1418.
- [26] P. Küsgens, M. Rose, I. Senkovska, H. Fröde, A. Henschel, S. Siegle, S. Kaskel, *Microporous Mesoporous Mater.* **2009**, *120*, 325–330.
- [27] J. B. Decoste, G. W. Peterson, B. J. Schindler, K. L. Killips, M. A. Browe, J. J. Mahle, *J. Mater. Chem. A* **2013**, *1*, 11922–11932.
- [28] M. Todaro, A. Alessi, L. Sciortino, S. Agnello, M. Cannas, F. M. Gelardi, G. Buscarino, *J. Spectrosc.* **2016**, 8074297.
- [29] V. Colombo, S. Galli, H. J. Choi, G. D. Han, A. Maspero, G. Palmisano, N. Masciocchi, J. R. Long, *Chem. Sci.* **2011**, *2*, 1311–1319.
- [30] L. Heinke, M. Tu, S. Wannapaiboon, R. A. Fischer, C. Wöll, *Microporous Mesoporous Mater.* **2015**, *216*, 200–215.
- [31] I. Khay, G. Chaplais, H. Nouali, C. Marichal, J. Patarin, *RSC Adv.* **2015**, *5*, 31514–31518.
- [32] F. Tian, A. M. Mosier, A. Park, E. R. Webster, A. M. Cerro, R. S. Shine, L. Benz, *J. Phys. Chem. C* **2015**, *119*, 15248–15253.
- [33] S. Bhattacharyya, R. Han, J. Joshi, G. Zhu, R. P. Lively, K. S. Walton, D. S. Sholl, S. Nair, *J. Phys. Chem. C* **2019**, *123*, 2336–2346.
- [34] S. Bhattacharyya, R. Han, W. G. Kim, Y. Chiang, K. C. Jayachandrababu, J. T. Hungerford, M. R. Dutzer, C. Ma, K. S. Walton, D. S. Sholl, S. Nair, *Chem. Mater.* **2018**, *30*, 4089–4101.
- [35] V. Chernikova, O. Yassine, O. Shekhah, M. Eddaoudi, K. N. Salama, *J. Mater. Chem. A* **2018**, *6*, 5550–5554.
- [36] H. G. W. Godfrey, I. da Silva, L. Briggs, J. H. Carter, C. G. Morris, M. Savage, T. L. Easun, P. Manuel, C. A. Murray, C. C. Tang, M. D. Frogley, G. Cinque, S. Yang, M. Schröder, *Angew. Chem. Int. Ed.* **2018**, *57*, 14778–14781; *Angew. Chem.* **2018**, *130*, 14994–14997.
- [37] A. J. Howarth, Y. Liu, P. Li, Z. Li, T. C. Wang, J. T. Hupp, O. K. Farha, *Nat. Rev. Mater.* **2016**, *1*, 14018.
- [38] S. Bhattacharyya, S. H. Pang, M. R. Dutzer, R. P. Lively, K. S. Walton, D. S. Sholl, S. Nair, *J. Phys. Chem. C* **2016**, *120*, 27221–27229.
- [39] M. Savage, I. Da Silva, M. Johnson, J. H. Carter, R. Newby, M. Suyetin, E. Besley, P. Manuel, S. Rudić, A. N. Fitch, C. Murray, W. I. F. David, S. Yang, M. Schröder, *J. Am. Chem. Soc.* **2016**, *138*, 9119–9127.
- [40] M. Savage, Y. Cheng, T. L. Easun, J. E. Eyley, S. P. Argent, M. R. Warren, W. Lewis, C. Murray, C. C. Tang, M. D. Frogley, G. Cinque, J. Sun, S. Rudić, R. T. Murden, M. J. Benham, A. N. Fitch, A. J. Blake, A. J. Ramirez-Cuesta, S. Yang, M. Schröder, *Adv. Mater.* **2016**, *28*, 8705–8711.
- [41] M. Morita, T. Ohmi, E. Hasegawa, M. Kawakami, M. Ohwada, *J. Appl. Phys.* **1990**, *68*, 1272–1281.

Manuscript received: May 30, 2019

Revised manuscript received: July 12, 2019

Accepted manuscript online: July 23, 2019

Version of record online: September 13, 2019